JOURNAL OF THE KOREAN ASTRONOMICAL SOCIETY
27: 13 ~ 29, 1994

THE SMOOTHED PARTICLE HYDRODYNAMICS AND THE BINARY TREE COMBINED INTO BTSPH: PERFORMANCE TESTS

KIM, W.-T., HONG, S. S. AND YUN, H. S.
Department of Astronomy, Seoul National University, Seoul 151-742, Korea
(Received Mar. 11, 1994; Accepted Mar. 25, 1994)

ABSTRACT

We have constructed a 3-dim hydrodynamics code called BTSPH. The fluid dynamics part of the code is based on the smoothed particle hydrodynamics (SPH), and for its Poisson solver the binary tree (BT) scheme is employed. We let the smoothing length in the SPH algorithm vary with space and time, so that resolution of the calculation is considerably enhanced over the version of SPH with fixed smoothing length. The binary tree scheme calculates the gravitational force at a point by collecting the monopole forces from neighboring particles and the multipole forces from aggregates of distant particles. The BTSPH is free from geometric constraints, does not rely on grids, and needs arrays of moderate size. With the code we have run the following set of test calculations: one-dim shock tube, adiabatic collapse of an isothermal cloud, small oscillation of an equilibrium polytrope of index 3/2, and tidal encounter of the polytrope and a point mass perturber. Results of the tests confirmed the code performance.

Key Words : numerical astrophysics, SPH, binary tree

I. INTRODUCTION

Understanding gas dynamical evolutions of astronomical objects often involves computer simulations. Numerical methods based on the Eulerian scheme are used for solving problems of well defined geometry. To treat systems of irregular shape, like interstellar clouds, the grids and finite differencing necessary for the Eulerian scheme require computer memory to be excessively large, which makes the Eulerian approach generally be limited to the problems of 2 and 2.5 dimensions. On the other hand, particle schemes of Lagrangian approach are not much constrained by the geometry. The smoothed particle hydrodynamics (SPH) (Lucy 1977; Gingold and Monaghan 1977) uses a fully Lagrangian scheme. It was developed for the very purpose to overcome the geometric constraint of the Eulerian scheme. Ever since numerical tests (Gingold and Monaghan 1980; Durisen, Gingold, Tholine and Boss 1987) were reported for the SPH, it has become one of the most versatile tools for gas dynamical problems in astrophysics (Benz 1990; Monaghan 1992).

In the SPH algorithm, continuous distribution of fluid is modeled by weighted sum of discrete particles. To effect the weighted summing properly with a reasonably small number of particles, the SPH introduces weighting kernel with parameter h called the smoothing length. The kernel is designed in such a way that when physical properties at a position are calculated, only those particles residing within $\sim h^3$ centered at the position are to be included in the weighted sum. The smoothing length could be fixed at the mean separation of particles, which may be a function of time. Use of such time dependent but spatially fixed value of smoothing length wouldn't cause any serious difficulties for systems more or less uniform. However, for systems having large density contrasts, it would over-estimate densities at locations where there are only a few particles within $\sim h^3$;

while it would under-estimate densities at locations of high density.

Dr. J.J. Monaghan was kind enough to make one of his earlier SPH versions available for us. This version employed spatially fixed smoothing length. But we became to have interests in collsions of interstellar clouds, which involve large density contrasts. As a gravity solver the version used multi-grid method, which mars the Lagrangian nature of the SPH by requiring grids. Fine griddings were necessary for our problems of cloud collision. We thus decided to make the smoothing length vary with position and time, and to replace the gravity solver from the multi-grid method to one retaining the Lagrangian nature.

The simplest particle method for gravity would be the direct N-body summation. But it becomes prohibitively expensive for system having large number of particles, because the number of operations per time step increases with particle number N as $\sim N^2$. The method of hierarchical tree (Barnes and Hut 1986; Hernquist 1987, 1990) and the method of binary tree (Jernigan 1985; Press 1987; Benz 1988; Benz, Bower, Cameron, and Press 1990) do not need gridding. In the tree schemes the number of operations per time step increases as $\sim N \log N$. Once the hierarchical tree and the SPH were combined into TREESPH by Hernquist and Katz (1988), it became a powerful particle method for solving astrophysical problems of gas dynamics. But in order to make the TREESPH play its full power, we need supercomputers. Although the binary tree scheme is not clearly vectorizable, it does have some advantages on scalar machines. We thus decided to use the binary tree as our gravity solver.

We have revised the version of SPH from Dr. Monaghan by making the smoothing length vary with position, and combined the resulting SPH with the binary tree. Thus has emerged a three-dimensional hydrodynamics code, named BTSPH. We have done a set of performance tests for the code. This paper presents the test results. In § II we briefly explain basic concepts of the SPH and specify what modifications we made to the version of SPH with fixed h. In §III we explain how the binary tree algorithm was incorporated into the BTSPH. In §IV we present results of the performance tests in details. In § V we summarize the paper.

II. HYDRO-PART OF THE BTSPH

1. Basic Equations

In the SPH algorithm, true density $\rho(\vec{r}_i)$ at position $\vec{r}_i$ is replaced by weighted mean ρ_i of neighboring particle masses:

$$\rho(\vec{r}_i) \simeq \rho_i \equiv \sum_{j=1}^{N} m_j W_{ij}, \tag{1}$$

where m_j stands for the particle mass at position $\vec{r}_j$, and W_{ij} is a suitably chosen weighting function. The same type of weighted sum approximates the values of all the physical properties. For the weighting function, we take the form suggested by Hernquist and Katz (1989),

$$W_{ij} = \frac{1}{2}[W(|\vec{r}_i - \vec{r}_j|, h_i) + W(|\vec{r}_i - \vec{r}_j|, h_j)], \tag{2}$$

and keep it to be symmetric with respect to i and j. The kernel $W(r, h)$ should be maximized at $r=0$, differentiable, and satisfy normalization condition $\int W(r-r', h)\, d^3r' = 1$. For the kernel the BTSPH employes the form suggested by Monaghan and Lattanzio (1985),

$$W(s, h) = \frac{1}{\pi h^3} \begin{cases} 1 - \frac{3}{2}\left(\frac{s}{h}\right)^2 + \frac{3}{4}\left(\frac{s}{h}\right)^3, & 0 \le \frac{s}{h} \le 1, \\ \frac{1}{4}\left[2 - \left(\frac{s}{h}\right)\right]^3, & 1 \le \frac{s}{h} \le 2, \\ 0, & \text{otherwise.} \end{cases} \tag{3}$$

When this kernel is used, the result of the weighted sum becomes second order accurate, $\rho(\vec{r}_i)=\rho_i+O(h^2)$ (Monaghan 1985; Hernquist and Katz 1989). Even though different values of smoothing length are assigned to different particles, the symmetric kernel conserves mass. Because the kernel function has to be calculated repeatedly, we save the function values in a table and interpolated them.

In the SPH algorithm, gas dynamical part of the force acting on particle i is calculated by

$$\overrightarrow{F_{Si}}=-m_i\sum_{j=1}^{N}m_j\left[\left(\frac{p_i}{\rho_i^2}+\frac{p_j}{\rho_j^2}\right)+\Pi_{ij}\right]\nabla_i W_{ij}. \tag{4}$$

Here the Π_{ij} term arises from the artificial viscosity. When adiabatic equation of state is assumed, pressure p_i is determined from specific internal energy u_i by

$$p_i=(\gamma-1)\sum_{j=1}^{N}m_j u_j W_{ij}, \tag{5}$$

where γ is the ratio of specific heats.

The artificial viscosity is introduced to prevent particles from penetrating each other, and we adopt for Π_{ij} the form suggested by Monaghan (1989):

$$\Pi_{ij}=\frac{-\alpha\mu_{ij}c_{ij}+\beta\mu_{ij}^2}{\rho_{ij}}, \tag{6}$$

with $\rho_{ij}=(\rho_i+\rho_j)/2$, $c_{ij}=(c_i+c_j)/2$, and c_i being local sound speed $(\gamma p_i/\rho_i)^{1/2}$. For contracting pair of particles, namely, $(\vec{v}_i-\vec{v}_j)\cdot(\vec{r}_i-\vec{r}_j)<0$, μ_{ij} is given by

$$\mu_{ij}=\frac{(\vec{v}_i-\vec{v}_j)\cdot(\vec{r}_i-\vec{r}_j)}{h_{ij}(|\vec{r}_i-\vec{r}_j|^2/h_{ij}^2+\eta^2)}, \tag{7}$$

with $h_{ij}=(h_i+h_j)/2$; while for expanding pair, $(\vec{v}_i-\vec{v}_j)\cdot(\vec{r}_i-\vec{r}_j)\geq 0$, μ_{ij} is set to be zero. According to Monaghan (1992), the following set of parameters describes the shock wave fairly well: $\eta\approx 10^{-2}$, $\alpha=1$, and $\beta=2$.

The SPH describes the first law of thermodynamics as

$$\frac{du_i}{dt}=\frac{1}{2}\sum_{j=1}^{N}m_j\left[\left(\frac{p_i}{\rho_i^2}+\frac{p_j}{\rho_j^2}\right)+\Pi_{ij}\right](\vec{v}_i-\vec{v}_j)\cdot\nabla_i W_{ij}. \tag{8}$$

The artificial viscosity is again given by equation (6), and the remaining terms are for the PdV work. When the system maintains isothermal condition, we do not have to solve this energy equation.

We now move particles according to

$$\dot{\vec{r}}_i=v_i, \tag{9}$$

and

$$m_i\dot{\vec{v}}_i=\overrightarrow{F_{Si}}+\overrightarrow{F_{Gi}}. \tag{10}$$

The local pressure gradient force $\overrightarrow{F_{Si}}$ is obtained from equation (4), and as will be explained shortly, the self-gravity force $\overrightarrow{F_{Gi}}$ is calculated by the method of binary tree.

If notice is made to $\nabla_i W_{ij}=-\nabla_j W_{ij}=-\nabla_j W_{ji}$, one may realize that equation (4) is anti-symmetric with respect to i and j. The anti-symmetry is intentionally kept in the SPH algorithm to ensure the conservations of total momentum and energy; their values calculated at each time step will thus serve a good measure of numerical accuracy.

2. Spatially and Temporally Varying Smoothing Length

Since spatial resolution of the SPH calculation is controlled by the smoothing length, it is important to know how to assign values for the length. When summations like equation (1) calculate weighted means of any physical properties at a point, the kernel function (equation [3]) excludes those particles that lie outside a $2h$ radius sphere centered at the point. If h is taken constant all through the system, waste of information is inevitable in regions of high density. This results in a degradation of resolution, and makes the weighted mean under-estimated. On the other hand, in regions of such low densities that only one particle may reside within the $2h$ radius sphere, the weighted mean becomes over-estimated. To overcome these difficulties, the smoothing length of each particle should be adjusted according to local density.

As a guide for making the necessary adjustment, Miyama, Hayashi, and Narita (1984) kept $\rho_i^{(n-1)}[h_i^{(n)}]^3$ to be a constant of time step. Here, the superscript in parentheses means the time step. As Benz (1990) pointed out, this way of adjusting h requires information at previous time step, and often brings about big changes of smoothing length over consecutive time steps. To avoid such sudden changes, Benz (1990) and Benz and Hills (1992) adjusted the time variation of h according to the following relation: $d\ln h/dt=(1/3)\nabla\cdot\vec{v}$. This approach looks physically sound, but requires $\nabla\cdot\vec{v}$ be calculated at each time step.

Hernquist and Katz (1989) compromised the two approaches, and determined at each time step the smoothing length $h_i^{(n)}$ of each particle by using the following relation:

$$h_i^{(n)}=h_i^{(n-1)}\left(\frac{1}{2}\right)\left[1+\left(\frac{N_\infty}{N_i^{(n-1)}}\right)^{1/3}\right], \tag{11}$$

where $h_i^{(n-1)}$ is the smoothing length at time step n-1, $N_i^{(n-1)}$ denotes the number of particles included in the weighted sum for local property, and N_∞ is an input parameter. The number 1 within the square brackets is designed to avoid sudden changes in the resulting smoothing length. As computations progress (n$\rightarrow\infty$), $N_i^{(n)}$ converges to N_∞. Actual value for N_∞ is to be determined in a trial-and-error fashion. Our trial calculations with total 3,400 particles suggested $N_\infty\simeq 35$ a reasonable choice (e.g. Goodman and Hernquist 1991).

3. Implementation of Time Evolution

For numerical stability, time and grid intervals should satisfy the Courant condition. In the SPH lagorithm h_i acts like the grid interval in the finite difference scheme. For the time step, δt, we use the criteria suggested by Monaghan (1989):

$$\delta t=0.2\min\left(\delta t_1,\ \delta t_2\right), \tag{12a}$$

where

$$\delta t_1=\min_i\left(\frac{h_i}{c_i+1.2\alpha c_i+1.2\beta\ \max_j\mu_{ij}}\right) \tag{12b}$$

and

$$\delta t_2=\min_i\left(|h_i/\dot{\vec{v}}_i|^{1/2}\right). \tag{12c}$$

The resulting time step is further kept smaller than some maximum value, *i.e.* $\delta t\leq\delta t_{max}$.

To integrate equations (9), (10), (4) and (8), the BTSPH employs a predictor-corrector scheme, which is second order accurate in time (Lattanzio and Henriksen 1988). At each time step, velocity and position of each particle are predicted at half step forward by

$$\begin{aligned} v_{i,p}^{(n+1/2)}&=v_i^{(n)}+\frac{\delta t_n}{2}f_i\left(r_{i,p}^{(n-1/2)},\ v_{i,p}^{(n-1/2)}\right),\\ r_{i,p}^{(n+1/2)}&=r_i^{(n)}+\frac{\delta t_n}{2}\left[v_{i,p}^{(n+1/2)}+v_i^{(n)}\right], \end{aligned} \tag{13}$$

where subscript p indicates predicted value, and f_i is net acceleration (gravity plus pressure gradient) acting on particle i. After calculating the acceleration with the information of predicted position and velocity, we correct the preditions as

$$\begin{aligned} v_{i,c}^{(n+1/2)} &= v_i^{(n)} + \frac{\delta t_n}{2} f_i \left(r_{i,p}^{(n+1/2)},\ v_{i,p}^{(n+1/2)} \right), \\ r_{i,c}^{(n+1/2)} &= r_i^{(n)} + \frac{\delta t_n}{2} v_{i,c}^{(n+1/2)}. \end{aligned} \tag{14}$$

Now the velocity and position at time step n+1 become

$$\begin{aligned} v_i^{(n+1)} &= 2 v_{i,c}^{(n+1/2)} - v_i^{(n)}, \\ r_i^{(n+1)} &= 2 r_{i,c}^{(n+1/2)} - r_i^{(n)}. \end{aligned} \tag{15}$$

(Not to make notations too complicated, we have dropped vector signs from vector quantities in the above three sets of equations.)

In this scheme of integration, the force is calculated only once per time step. This is an advantage, because force calculation needs time most. Here, we may note that this scheme conserves the total angular momentum within $O(\delta t^4)$.

III. GRAVITY SOLVER OF THE BTSPH

It is the Poisson part that costs most. There are algorithms which are faster than the direct N-body sum. For example, FFT-based convolution method and multi-grid method are proved to be very efficient. But they all need grids in either the Fourier or real space. In collision simulations, however, particles are often ejected at large distances; and to cover all the particles, these methods would require grid of an excessively large size. Furthermore, if we incorporate these methods with the SPH, the grid cell should be smaller than the minimum smoothing length. Therefore, the grid-based Poisson solvers will lose their merits in the variable h version of SPH.

Furthermore, when a grid method is used with the SPH, we have to calculate the density at a grid point by interpolating densities at neighboring particle positions. This is because the SPH data are not on regularly spaced three dimensional grids but on particles. After calculating the gravitational potential from the interpolated densities at the grid points, we must re-interpolate the corresponding gravitational force back to the individual particles. To maintain accuracy in the two step interpolation, finer grids are required particularly at regions of rapid density variation. Therefore, the grid-based methods are disadvantageous for such problems as cloud collision.

Since the method of hierarchical tree can fully be vectorized (Hernquist 1990), it becomes powerful on supercomputers. Although the method of binary tree (BT) is not clearly vectorizable, it has some advantages on scalar machines (Benz 1988). Because the total number of nodes is always $2N-1$ in the BT scheme, there are no needs for surplus arrays, which reduces the code size significantly. In the method of hierarchical tree, two closely neighboring particles could be housed in two different cells. However, in the BT scheme, neighboring particles are always grouped into one (Benz, Bower, Cameron, and Press 1990). We thus decided to employ the binary tree as our gravity solver. For details of the method we refer readers to Press (1987) and Benz *et al.* (1990). In what follows we will briefly explain how the binary tree scheme is incorporated into the BTSPH.

For each particle we first determine its nearest neighbor. The mutually nearest neighbors are then replaced by a second level node. The unpaired single particles and the newly made nodes enter the nearest neighbor searching algorithm to look for the mutually nearest neighbors again, which become third level nodes; and so on. (Individual particles can be considered as nodes on the lowest level.) On each level, the newly made node is characterized by mass M, position $\vec{R}$, and quadrupole moment tensor $\mathbf{Q}$, which are determined from the same

properties of the two lower level partners. Let us denote by m_1, m_2, $\vec{r}_1$, $\vec{r}_2$, $\mathbf{Q}_1$ and $\mathbf{Q}_2$ the masses, positions, and quadrupole moment tensors of partners 1 and 2 of a node. The corresponding properties of the node resulting from the partners 1 and 2 are given by

$$M = m_1 + m_2, \tag{16a}$$

$$\vec{R} = \frac{m_1 \vec{r}_1 + m_2 \vec{r}_2}{M}, \tag{16b}$$

and

$$\mathbf{Q} = \mathbf{Q}_1 + \mathbf{Q}_2 + \frac{m_1 m_2}{M} (\vec{r}_2 - \vec{r}_1) \otimes (\vec{r}_2 - \vec{r}_1). \tag{16c}$$

If two partners are the lowest level particles, both $\mathbf{Q}_1$ and $\mathbf{Q}_2$ are zeros; if one of them is a particle, its $\mathbf{Q}$-value should be zero. Equation (16b) means that a node is positioned at the center of mass of its two partners, and equation (16c) is the parallel-axis theorem in the classical dynamics. In addition to $\vec{R}$, $\mathbf{Q}$, and M, a full description of the binary tree requires us to calculate the convergence radius, $\Re$. It is the radius of a sphere, outside which one can be confident that multipole expansion for gravitational force is convergent. As a conservative estimate of the convergence radius we will take (Benz *et al.* 1990).

$$\Re = \max\left(\frac{m_1}{M}|\vec{r}_2 - \vec{r}_1| + \Re_2, \frac{m_2}{M}|\vec{r}_2 - \vec{r}_1| + \Re_1\right). \tag{17}$$

When the binary tree is fully constructed, the gravitational force acting on each particle is calculated by the multipole expansion. The nodes inside a few times the convergence radius, $(1.0 \sim 1.6)\Re$, from a given particle should be all opened up. And all the particles consisting the opened-up nodes exert monopole forces on the given particle. The monopole force is calculated simply by

$$\overrightarrow{F_{G_i}} = m_i \sum_{j=1}^{jmx} m_j \vec{r} f(r), \tag{18}$$

where $f(r) = Gr^{-3}$ with G being the gravitational constant, $\vec{r} = \vec{r}_j - \vec{r}_i$ win. r being the distance between two particles i and j, and jmx means the number of all the opened-up node particles. The gravitational forces due to the remaining nodes that are not opened are now calculated by the multipole expansion up to quadrupole moment. Due to a node with parameters M and $\mathbf{Q}$, a particle of mass m will experience gravitational acceleration given by

$$\frac{\overrightarrow{F_G}}{m} = Mf(r)\vec{r} + \frac{f'(r)}{r}\mathbf{Q}\cdot\vec{r} + \frac{1}{2}\left[\frac{f''(r)}{r^2}\vec{r}\cdot\mathbf{Q}\cdot\vec{r} + \frac{f'(r)}{r}\left(\mathrm{tr}\,\mathbf{Q} - \frac{\vec{r}\cdot\mathbf{Q}\cdot\vec{r}}{r^2}\right)\right]\vec{r}, \tag{19}$$

where derivatives of $f(r)$ are with respect to r.

When the interparticle distance is very small, evaluation of the monopole force by equation (18) needs softening. In the BTSPH we use the spline kernel suggested by Hernquist and Katz (1989) to soften:

$$f(r) = \begin{cases} \varepsilon^{-3}\left(\frac{4}{3} - \frac{6}{5}q^2 + \frac{1}{2}q^3\right); & 0 \le q < 1, \\ r^{-3}\left(-\frac{1}{15} + \frac{8}{3}q^3 - 3q^4 + \frac{6}{5}q^5 - \frac{1}{6}q^6\right); & 1 \le q < 2, \\ r^{-3}; & \text{otherwise}, \end{cases} \tag{20}$$

where $q \equiv r/\varepsilon$. For softening parameter, ε, we choose the smoothing length of the particle, h_i. Since equation (20) has to be calculated many times, it is wise to save the results in a table.

IV. PERFORMANCE TESTS FOR THE BTSPH CODE

In order to see how well the code works, we have performed the following set of test calculations: (i) one dimensional shock tube, (ii) adiabatic collapse of an isothermal cloud, (iii) oscillation of an equilibrium polytrope, and finally, (iv) tidal encounter of an equilibrium polytrope with a point mass. This section presents the test results.

1. Riemann Shock Tube Calculation

The one-dimensional Riemann shock tube problem of Sod (1978) is considered a standard test for hydrodynamics code. The initial conditions are the same ones of Monaghan and Gingold (1983):

$$\begin{cases} \rho_L = 1.00,\ p_L = 1.0000,\ v_L = 0;\ x \le 0, \\ \rho_R = 0.25,\ p_R = 0.1795,\ v_R = 0;\ x > 0. \end{cases} \tag{21}$$

The smoothing length was fixed and the time step was determined by equation (12). The ratio of specific heats is $\gamma = 1.4$. Initially we arranged 5,000 equal-mass particles in the range, $-1.0 \le x \le 1.0$, in such a way that they depict the situation given in equation (21). We tried several sets of viscosity coefficients.

The resulting distributions of density ρ, velocity V_x, thermal energy U, and pressure P at time t=0.15 are shown in Fig. 1, where dots represent the numerical results and lines are for the analytical solutions obtained by standard techniques (e.g. Courant and Friedrichs [1956]; Rasio and Shapiro [1991]). The viscosity parameters used to get this set of results are $\alpha = 1$, $\beta = 2$, and $\eta = 0.01$.

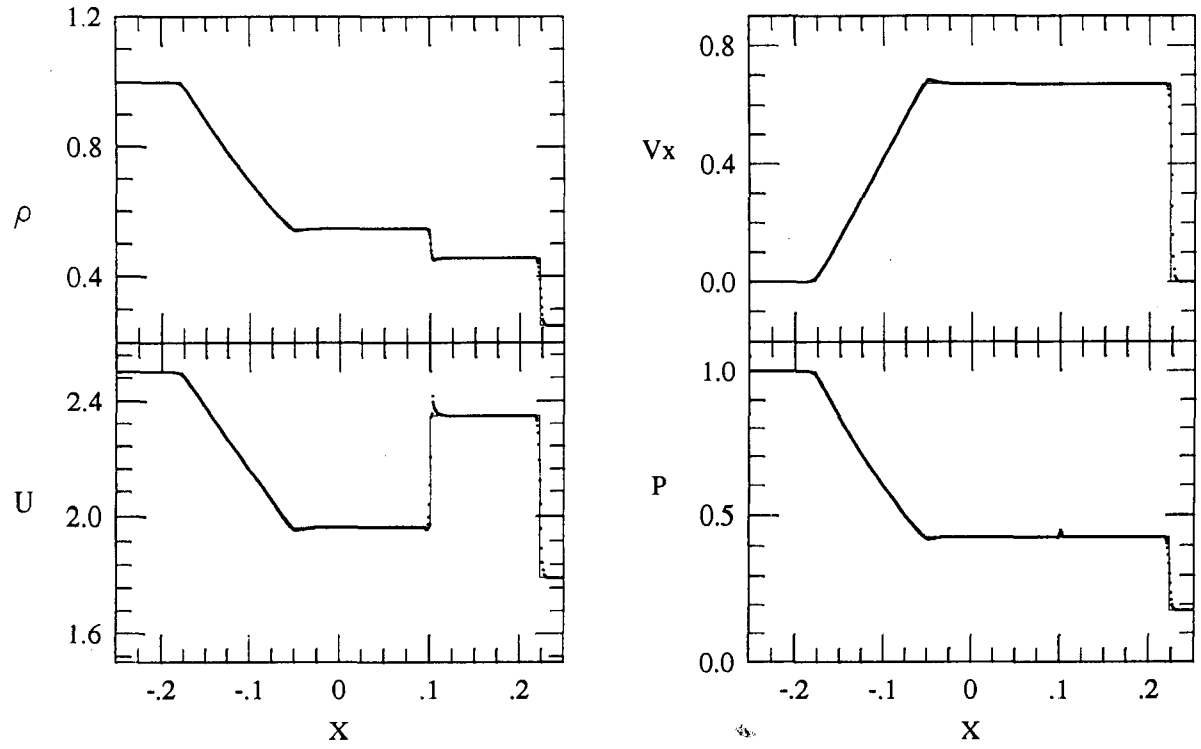

Fig. 1. One-dim shock tube test. Variations of density ρ, velocity V_x, specific thermal energy U, and pressure P at time t=0.15 are shown as functions of position x. Dots represent the results of numerical simulation, and solid lines are for the results of analytical solutions.

The discontinuity at x$\simeq$0.22 is smeared over $\Delta x \simeq 3h$. This resolution is comparable to the one from finite -difference code (Sod 1978). If we reduce α and β, the resolution will further improve, but at the risk of having postshock oscillations. Because the artificial viscosity does not affect particles in expanding motion, the structure of the rarefaction wave is independent of the viscosity parameters. The one dimensional test with several sets of viscosity parameters has led us to confirm that $\alpha=1$ and $\beta=2$ are reasonable choices.

2. Adiabatic Collapse of an Isothermal Cloud

With our BTSPH we have followed the collapse of an isothermal cloud. The same test was done by Thomas (1987) with one-dimensional Lagrangian code of finite difference scheme, by Evrard (1988) with P3MSPH, and by Hernquist and Katz (1989) with TREESPH. To make comparison easy we took the same initial conditions as theirs. The density profile is given by

$$\rho(r)=\frac{M}{2\pi R^2}\frac{1}{r}, \tag{22}$$

where M is the total mass and R the initial radius of the sphere. The gas sphere was initially isothermal with specific internal energy $U=0.05GM/R$ and $\gamma=5/3$. In total 3,544 equal-mass particles were first placed on regular grids, and we then moved them to mimic the given density profile. We let equation (11) with $N_\infty=40$ calculate the smoothing length, and took $\alpha=1$ and $\beta=2$ again. For the time step we used equation (12) with $\delta t_{max}=0.022$ in this case.

We have monitored various energies from t=0.0 to 2.3, and Fig. 2 shows their time variations. Here the system of units is G=M=R=1. The initial imbalance between self-gravity and pressure gradient makes the gas cloud collapse slowly. The collapsing motion gets accelerated as the density builds up toward the center. The kinetic energy E_{kin} associated with the collapsing motion is converted into the thermal energy E_{thr} at time around t$\simeq$1, when the cloud is compressed most. The accumulated thermal energy decelerates the collapse and eventually reverses its direction. As time goes on, the cloud approaches virial equilibrium. The total energy E_{tot} is conserved within 0.04 percent.

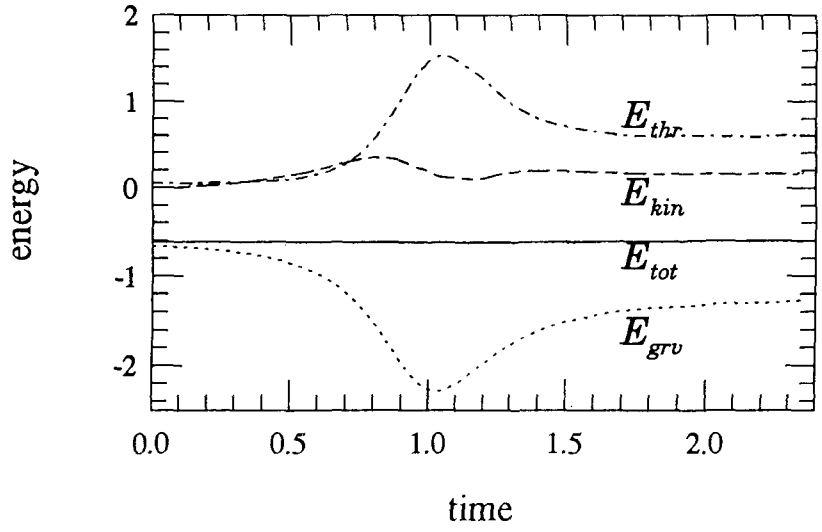

Fig. 2. Variations of the various energies with time. An initially isothermal cloud with $\rho(r)\propto 1/r$ and $\gamma=5/3$ undergoes an adiabatic collapse, and then expands until it reaches virial equilibrium. Time variations of total thermal E_{thr}, kinetic E_{kin}, and gravitational E_{grv} energies of the system are illustrated by dash-dotted, dashed, and dotted lines, respectively. The solid line represents the time variation of grand sum E_{tot} of the three total energies; in the scale of this figure, one can hardly notice any changes in E_{tot}. The conversion of the gravitational to the thermal energy becomes maximum after one free-fall time, when the system is most compressed.

Figure 3 describes how Mach number V_r/c, normalized density ρ/ρ_o, radial velocity V_r/V_o, and thermal energy U/U_o vary with radial distance r/R at three time epochs t=0.00 (solid line), 0.88 (dashed line), and 1.76 (dash-dotted line). The dashed line (t=0.88) in the frame of Mach number clearly shows the outwardly propagating shock develop in the region $0.18 \leq r/R \leq 0.5$. The frames of density and thermal energy demonstrate the development of core-envelop structure. The core part is nearly in isothermal condition; while the envelop region experiences adiabatic cooling as it expands. Our results are in good agreement with those by Thomas (1987), Evrard (1988), and Hernquist and Katz (1989). Since none of the four codes is based on the same numerical scheme, the agreement gives us strong confidence on the BTSPH.

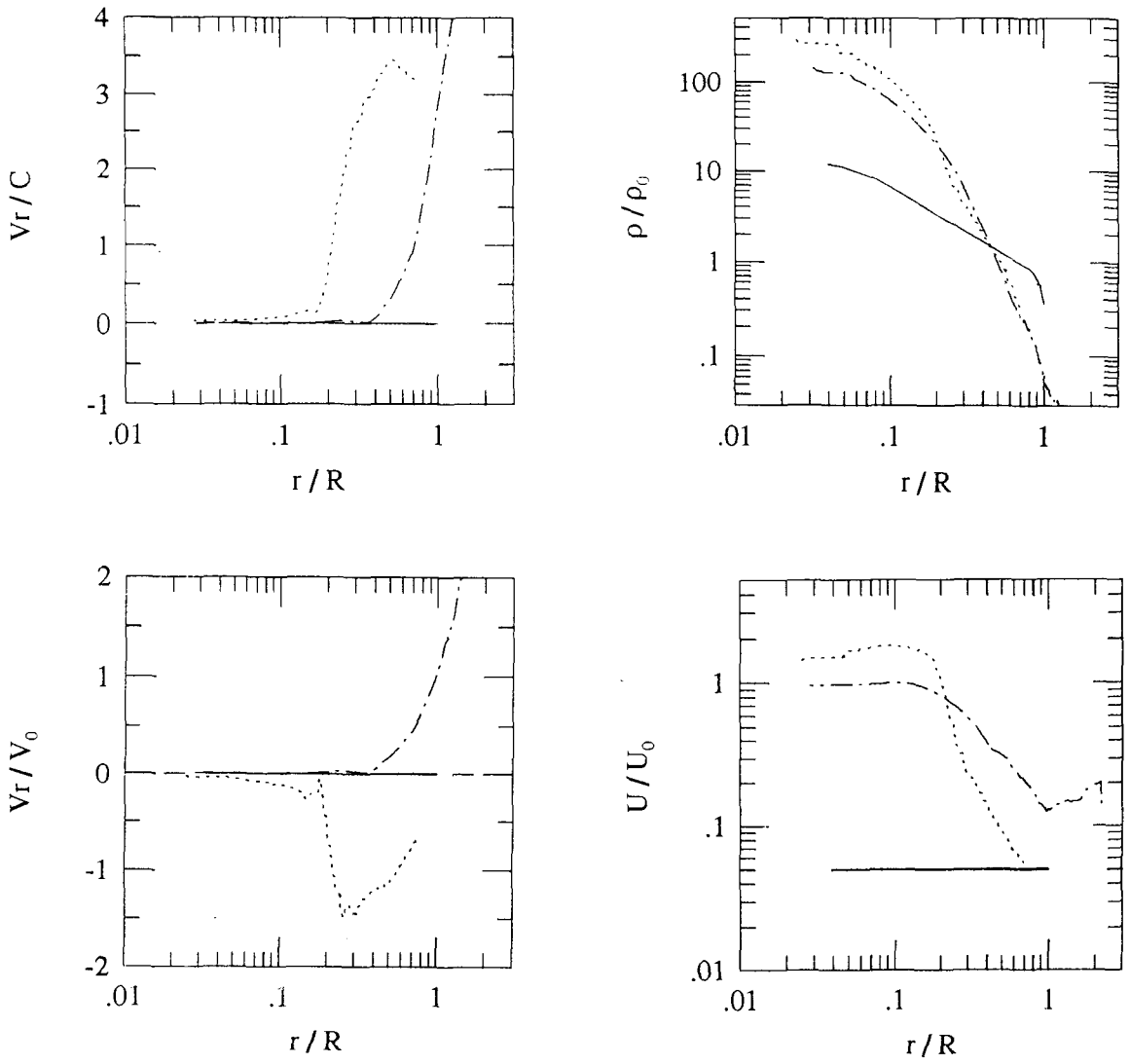

Fig. 3. Spatial profiles of radial velocity, Mach number of the radial velocity, density, and internal energy are presented at three epochs: solid, dotted, and dash-dotted lines are for the profiles attained at t=0.00, 0.88, and 1.76, respectively. As time goes on, the cloud develops core-envelope structure. The core is in isothermal condition, while the envelope has experienced cooling due to an adiabatic expansion.

The BTSPH does show some differences from the other three codes. In the velocity frame of Fig. 3 we can see small fluctuations at r/R=0.1~0.3. These were not seen from the results of TREESPH, and yet among the

three it is the one most similar to the BTSPH. The local fluctuations of velocity seem to have originated from the regularity in the initial particle distribution. Because we placed the particles regularly at 3-dim grid points, an extra force may have arisen from the geometrical regularity of the particle distribution. On the other hand, Hernquist and Katz (1989) placed the particles randomly by using an acceptance-rejection procedure, and they further smoothed the resulting velocity field and thermal energy. This could have substantially lessen possible peculiarities of the geometry.

Placing particles at grid points has merits, too. It is one of the easiest ways to model density profile accurately. Our profile agrees with equation (22) better than the profile of Hernquist and Katz (1989) does. In the central region, $0 \leq r/R \leq 0.1$, the BTSPH satisfies the isothermal condition much better than the TREESPH does. We think this is due to the better representation of the initial density profile.

3. Maintenance of a Polytrope in Equilibrium

We now test how well the BTSPH maintains an equilibrium polytrope in the state of hydrostatic equilibrium. We let random number generator locate 3,544 points within a sphere. At each point we calculate local density, the density a polytrope with index 3/2 would have at the point. To the point we then assign mass that is proportional to the local density. Equation (11) with $N_\infty = 40$ determines the smoothing length for each particle at each time step.

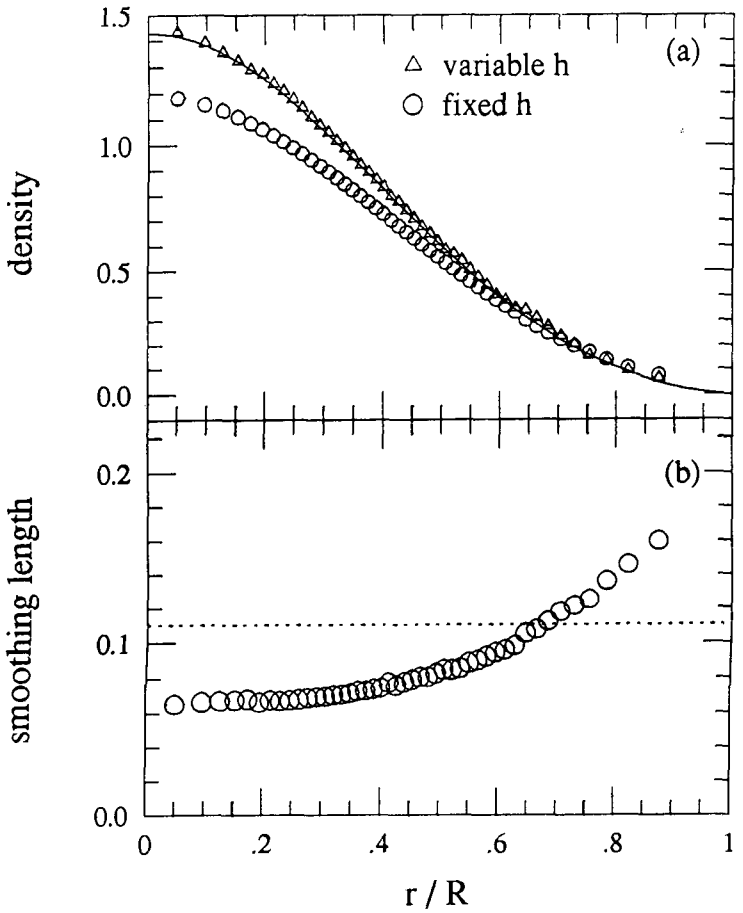

Fig. 4. Density profile of a polytrope of index 3/2 is modeled by using fixed h (dots) and varying h and particle mass (dashes) according to local density. In the upper frame of this figure, the two resulting profiles are compared with the true profile (solid line). The open circles in the lower frame illustrate how the smoothing length varies with radial distance, and the dashed line indicates the value of fixed h. In most part of the polytrope, the variable h reproduces the true profile much better than the fixed one does. However, both profiles tend to over-estimate the density near the cloud boundary.

The density profile (open triangles) modeled by using variable h is compared in Fig. 4a with the profile (open circles) obtained by fixed $h=(1/2)\ (N_\infty/N)^{1/3}\simeq 0.11$. The solid line in the figure is the analytical result from the Lane-Emden solution. Open circles in Fig. 4b represent the variation of h with radial distance, and the dashed line indicates the fixed h value. As expected, the weighted sum with variable smoothing length reproduced the radial density distribution more faithfully than that with fixed h does. The same can be said for the pressure gradient (Fig. 5) and the gravitational force (Fig. 6).

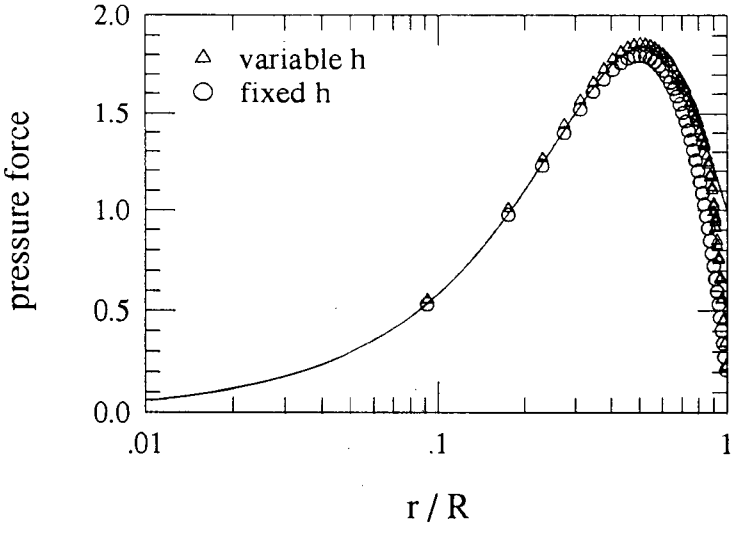

Fig. 5. Run of pressure gradient within an equilibrium polytrope of index 3/2 is calculated by using fixed h (dots) and varying h and particle mass (dashes), and the resulting gradient profiles are compared with the true gradient (solid line) obtained from the Lane-Emden function. The gradient calculated by the weighted sum could not quite reach the true gradient, regardless whether the smoothing length is varied or not.

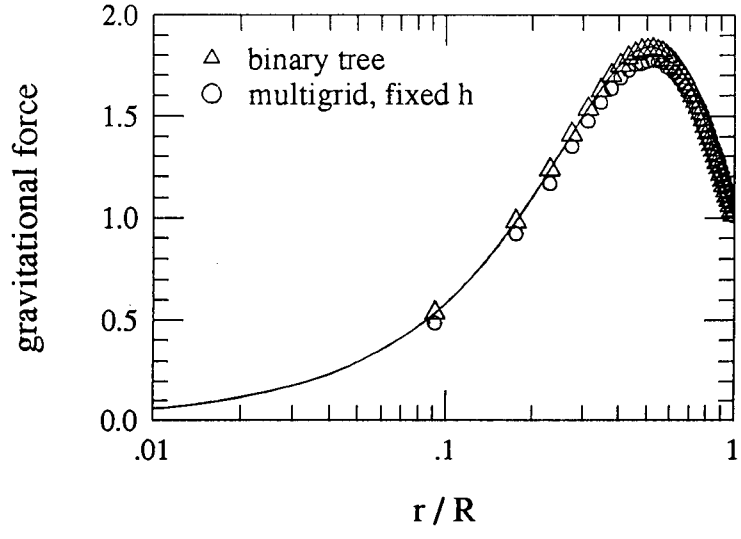

Fig. 6. Run of gravitational force within an equilibrium polytrope of index 3/2 is calculated by using the method of binary tree (dashes), and is compared with that by the multi-grid method with fixed h (dots). The analytical result obtained from the Lane-Emden solution is shown by the solid line. The multi-grid method with fixed h under-estimates the gravitational force everywhere. However, the method of binary tree almost perfectly reproduces the analytical result over the entire range of radial distance.

We computed the pressure gradient force by using variable h (dashes) and also by using fixed h (dots), and compared, in Fig. 5, the resulting distributions of the gradient with the analytical result (solid line). Except for the region near the cloud boundary, the gradient force computed with variable h accurately follows the analytical result. The calculated gradient has an error of 6.4 percent on the average; most of the 6.4 percent error comes from the region near the boundary. Because there are no particles outside the cloud, in the region $r/R \geq 0.8$ the weighted sum tends to over-estimate the density, which results in an under-estimation of the pressure gradient.

We also computed the self-gravitational force by the method of binary tree (dashes) and of multigrid with fixed h (dots). They are compared in Fig. 6 with the analytical result (solid line). In the entire region of the cloud, the result of binary tree follows the analytical one very accurately; relative error between the two is only 0.3 percent.

The two solid lines in Figs. 5 and 6 are exactly the same, because the polytrope is in equilibrium. The slight imbalance between the calculated pressure gradient (dashes) and the gravitational force (solid line) near the boundary initiates the collapsing motion. We have followed ensuing evolution of the polytrope from t=0 to 25. The polytrope oscillates around the equilibrium configuration with amplitude $\simeq h_i$. Figure 7 shows the oscillation resulted in the total thermal energy: relative amplitude and period of the oscillation are 0.93 percent and 3.96, respectively. Corresponding period of Theuns (1992) is ~4 and that of Lucy (1977) is 3.40. Of these three, our result is closest to the theoretically calculated value 3.82. Notice that the oscillation amplitude becomes smaller as time goes on. This is because the particles located initially on grid points move slowly to the positions of lower energy. The total energy is conserved within 0.1 percent.

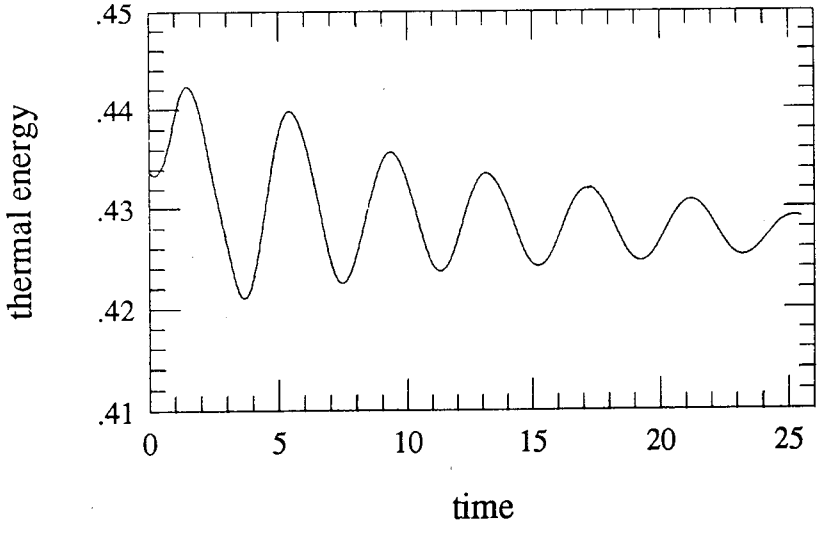

Fig. 7. The slight difference that can be seen between the dashes and the solid line in Fig. 5 or 6 provides an initial drive for the cloud to oscillate. As particles settle into positions of lower energies, the oscillation gets damped. The resulting change in the specific internal energy was monitored, and is shown as a function of time. Mean period of oscillation is found to be 3.96, which is close to the theoretically obtained value 3.82.

4. Tidal Encounter of the Polytrope with a Point Mass

Press and Teukolsky (1977) presented a theoretical method to calculate the amounts of orbital energy and angular momentum that are lost during an encounter between a main sequence star and a white dwarf. It is based on an expansion of the tidal perturbation in terms of the normal modes of non-radial oscillations. This was done in an effort to explain the X-ray sources in globular clusters (Fabian, Pringle and Rees 1975). and the

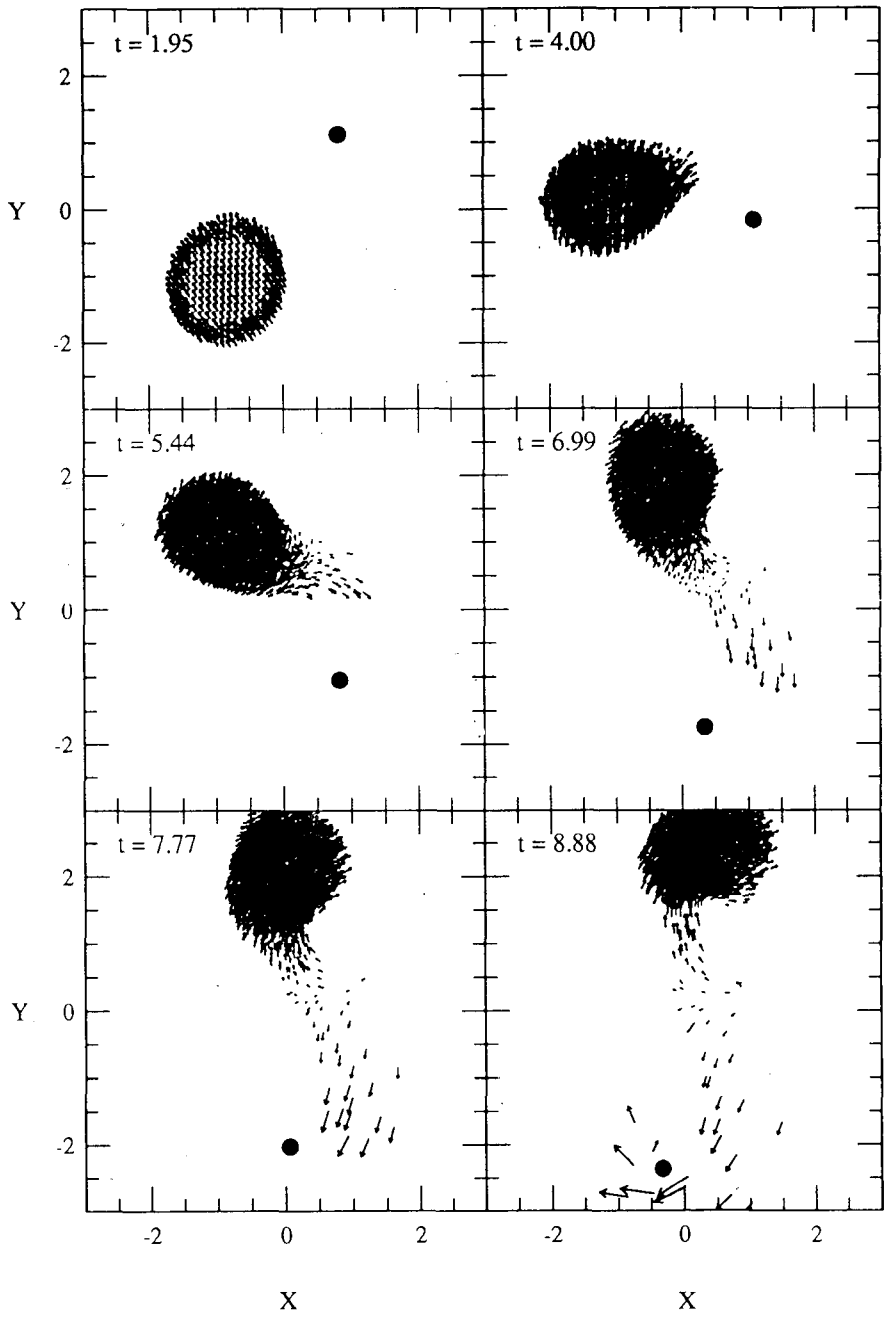

Fig. 8. Snapshots of the tidal encounter between an equilibrium polytrope of index 3/2 and a point mass perturber are shown at six time epochs, t=1.95, 4.00, 5.44, 6.99, 7.77, and 8.88. The fluid polytrope and the point perturber have the same mass. The perturber is shown by the small filled circle. Location and velocity of each fluid particle are projected onto the x-y plane, the plane of initial orbit. Origin of x and y coordinates is at the center of mass of the two-body system. The perturber approaches the polytrope in a parabolic orbit with initial periastron distance q=2.2 times the polytrope radius. Calculations start from the moment when the perturber is at distance 4 times the radius. The perturber reaches the periastron at time t≃3.5. Some time before the periastron passage, the polytrope starts a prograde rotation, and swells up toward the perturber, and the swollen-up part soon lags behind it. At time t≃7, a significant number of particles leave the polytrope; some of them fall back to the polytrope cloud and others are attached to the perturber.

calculations were later extended by several authors, for example, by Lee and Ostriker (1986), and by McMillan, McDermott, and Taam (1987). As a dynamical test for the BTSPH, we decided to simulate the tidal encounter of the n=3/2 polytrope with a point mass.

We used the same polytrope described in the last section. The system of units is such that G=R=M=1, where M and R are mass and radius of the polytrope. Initially a point perturber of mass m=1 was located at distance d=4 from the polytrope center. The perturber was given velocity appropriate for a parabolic orbit with the unperturbed periastron distance q in the range $1.8 \leq q \leq 2.6$.

Figure 8 shows the snapshots for the case q=2.2. In the figure the filled circle denotes the point perturber, and the extended body does the polytrope. All the particles consisting the polytrope are projected onto the x-y plane, whose origin is kept at the center of mass of the system. Both the polytrope and the perturber move clockwise. Some time before the point perturber comes to the periastron, a small portion of the polytrope swells up toward the point mass, but soon lags behind it. The lagging is natural, because the internal sound speed is smaller than the relative orbital velocity. After $t \simeq 7$ the polytrope experiences mass loss. Some of the mass moves toward the perturber, while the rest falls back to the polytrope.

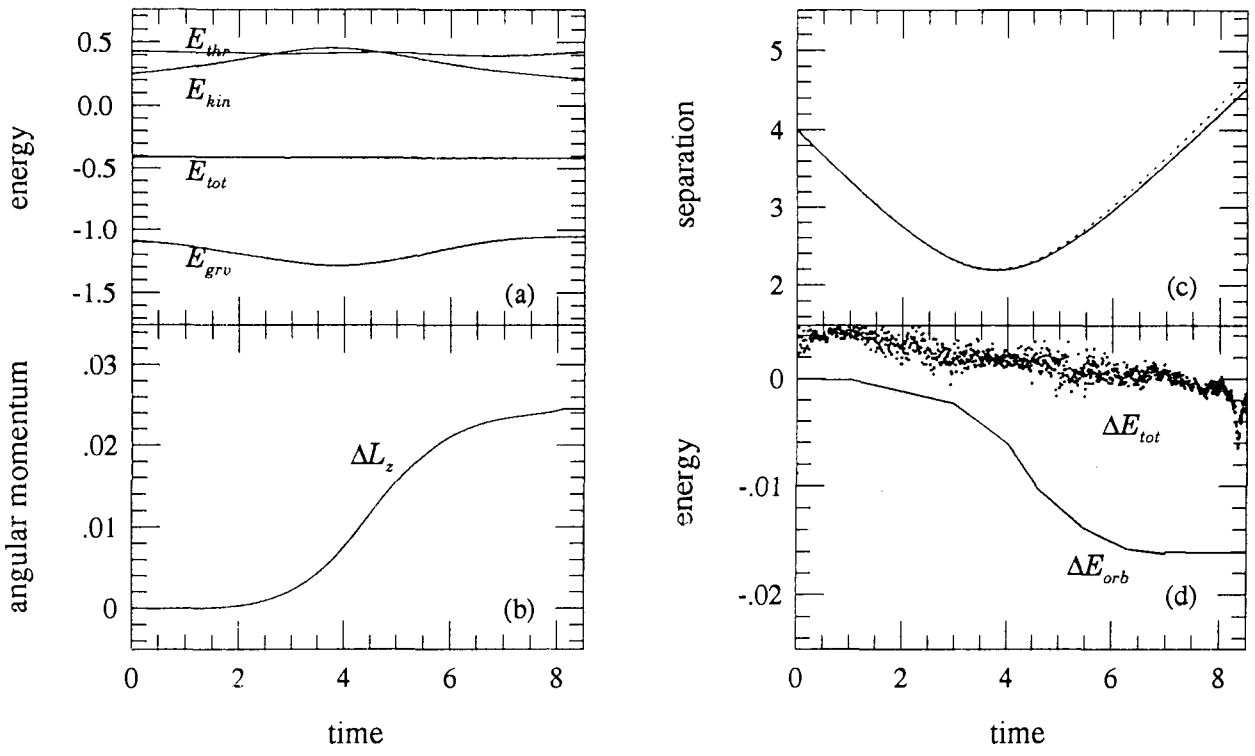

Fig. 9. Changes of the various energies, during an encounter between an equilibrium cloud of polytrope with index 3/2 and a point mass perturber, are monitored in frame *a*. Frame *b* of this figure illustrates how quickly the orbital angular momentum of the perturber is transferred to spin angular momentum of the polytrope. Rapid gain of the spin occurs when the perturber comes around the periastron, and the polytrope cloud rotates at a constant speed eventually. The net gain of the spin angular momentum after completion of the encounter depends on the periastron distance. In frame *c*, the dotted line shows how the separation between the point perturber and the polytrope center would vary with time, if there were no tidal interactions between the two. The actual separation is represented by the solid line, which reaches somewhat below the dotted line. This is because the perturber loses its orbital energy due to tidal interaction. The dots in frame *d* represent the time variation of the total energy. Since the total energy should be conserved throughout the encounter, the net change in the total energy is a measure of numerical accuracy. The solid line in the same frame illustrates how rapidly the orbital energy of the system is transferred to the rotational kinetic energy of the polytrope. Since the net change in the total energy is much less than that in the orbital energy, the numerical error is negligible in the net rotational energy gained by the polytrope.

Various energies have been monitored throughout the encounter, and their time variations are shown in Fig. 9a. By the tidal interaction, the orbital angular momentum of the perturber is transferred to the spin angular momentum of the polytrope. As shown in Fig. 9b, the spin angular momentum increases rapidly at times around the periastron passage, and then becomes finite as the perturber moves farther out. For the q=1.8 case, however, all the mass lost from the polytrope is attached to the point mass and goes with it.

At each time step we have calculated the distance between the point mass and the center of mass for all the fluid particles, and its time variation (solid line) is compared, in Fig. 9c, with that of the distance between two point masses moving in a true parabolic orbit (dashed line). The solid line departs from the dashed one from the moment t≃3.5. This is because the orbital kinetic energy of the point mass is gradually dissipated, as it approaches the periastron. The periastron distance is finally reduced to 2.19 from its original value 2.20.

We defined the orbital energy, $E_{orb}(t)$, of the polytrope and the point mass by

$$E_{orb}(t)=\frac{1}{2}\mu v_r^2+\Phi, \tag{23}$$

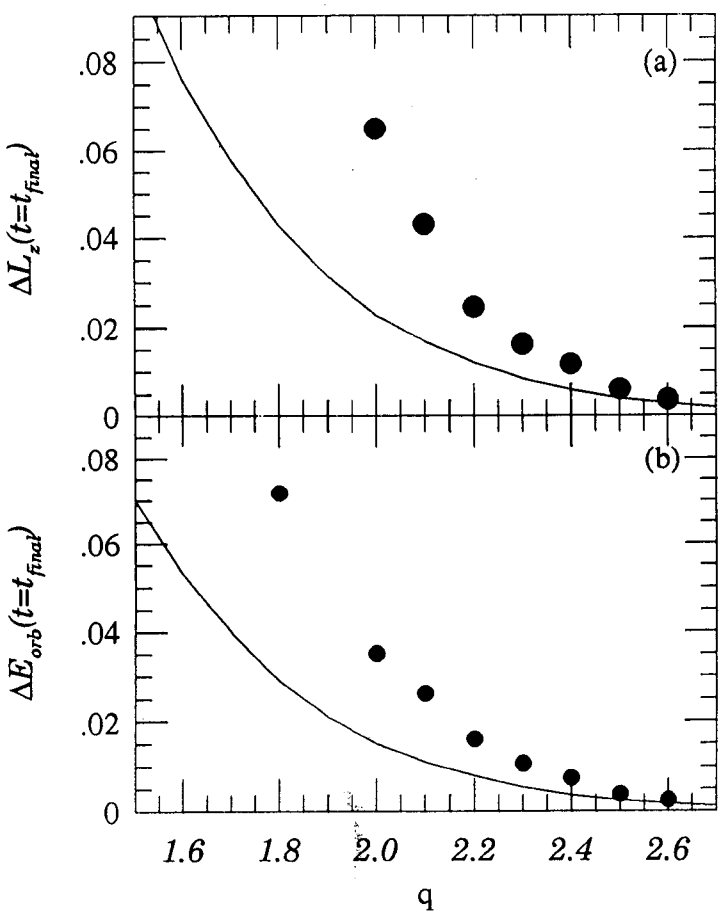

Fig. 10. Frame *a* of this figure shows how much of the orbital angular momentum the perturber has been transferred to the spin angular momentum of the polytrope cloud through the tidal encounter of given periastron distance q. Frame *b* does the same for the transfer of the orbital energy. Small filled circles are the results from the BTSPH simulations, and the solid lines are the theoretical results of linear analysis. The large difference between the simulation and the linear theory at small values of q indicates that non-linear effect dominates the tidal interaction in close encounters.

where μ is the reduced mass, v_r means the relative orbital velocity, and Φ represents the gravitational potential energy. Since M = 1 and m = 1, the reduced mass simply becomes 1/2. At each time step we have calculated the orbital energy. And change of the orbital energy, $\Delta E_{orb}(t) = E_{orb}(t) - E_{orb}(0)$, is shown in Fig. 9d as a function of time: when the perturber is near the periastron, the change is rapid.

Some of the orbital energy change is certainly due to numerical noise. Since the total energy E_{tot} of the system should remain constant throughout the encounter, its time variation is a good measure of the numerical accuracy. It is difficult to notice any variation in the total energy from the straight line in Fig. 9a. Instead we have calculated the change ΔE_{tot} in the total energy, and showed its time variation by dots in Fig. 9d. It is clear that the numerical errors are negligible for the change of orbital energy. As was the spin angular momentum, Fig. 9d demonstratess that the reduced amount of the orbital energy becomes constant as the perturber moves farther out.

It is interesting to know, as functions of periastron distance, the transferred amounts of the orbital to the spin angular momentum and energy. We have run simulations of encounters with different values of q, and evaluated the final amounts of the transferred orbital angular momentum $\Delta L_z (t \to \infty)$ and energy ΔE_{orb} $(t \to \infty)$. In Fig. 10 the results (filled dots) from the BTSPH simulations are compared with the ones (solid lines) from the linear analysis by Lee and Ostriker (1986).

The two results seem to agree for the encounters with large periastron distance. For distant encounters with $q > 2.6$, the net change in orbital energy becomes so small that it can hardly be differentiated from numerical noises. On the other hand, the smaller becomes q, the larger discrepancy is resulted between the numerical and analytical results. This is not because the BTSPH code faces limits in its performance, but because for such close encounters non-linear effects become important in the tidal interaction (Davies, Benz, and Hills 1991; Rasio and Shapiro 1991). The method based on linear analysis becomes invalid for such close encounters.

V. SUMMARY

The smoothed particle hydrodynamics and the method of binary tree have been combined into a three dimensional hydrodynamics code, called BTSPH. In this study we have done a set of performance tests for the code, and reached a conclusion that the code is satisfactory. In what follows the test results are summarized along with a few important attributes of the code.

By making the smoothing length vary with local density, we have improved not only spatial resolution but also dynamic range of the SPH calculations. One-dim shock tube tests have confirmed us that $\alpha = 1$, $\beta = 2$, and $\eta = 10^{-2}$ are the optimal values for the viscosity coefficients. By employing the method of binary tree as the Poisson solver, particle nature of the SPH scheme is kept intact in the BTSPH. The test done for the gravitational potential of an equilibrium polytrope of index 3/2 demonstrates that the method of binary tree calculates the gravitational force more accurately than the multi-grid method can do with fixed smoothing length.

With the BTSPH we have simulated an adiabatic collapse of an initially isothermal cloud. The code describes the mutual exchange among the gravitational, kinetic, and thermal energies of the cloud correctly, and conserves the total energy within four parts in ten thousands. The cloud is shown to develop the core-envelope structure. The core part is in isothermal state; while the envelope experiences adiabatic cooling as it expands. The cloud eventually enters a stage of virial equilibrium.

To check whether the BTSPH can maintain an equilibrium cloud in the state of equilibrium, we have followed the oscillation of a polytrope cloud of index 3/2. The total energy is conserved within one part in one thousand. The mean period of oscillation is found to be 3.96 times the free-fall time. We think this is close enough to 3.82, a theoretically obtained value, to conclude that the BTSPH indeed maintains an equilibrium polytrope in the state of equilibrium.

With the BTSPH we have simulated the tidal encounter of an equilibrium polytrope cloud of index 3/2 with a point perturber, both having the same mass. The results correctly describe the time variations and exchanges of the various energies. The BTSPH conserves the total energy of the system within a few percent throughout the encounter. The net amounts of the angular momentum and energy from the orbital to the spin motion are

calculated as functions of periastron distance and compared with the theoretical values of linear analysis. For close encounters with periastron distance less than ~2.5 times the cloud radius, the non-linear effect dominates the tidal interaction.

ACKNOWLEDGEMENTS

We are grateful to Dr. H. M. Lee, Dr. H. Kang, and Dr. J. J. Monaghan for making one of the SPH versions available for us, and Ms. H. S. Lee for her earlier contribution to this study. We are pleased to acknowledge the comments and corrections suggested by the referee. Facility for Astronomical Image Analysis at ICNSRF was used to make some of the calculations reported here and to process the resulting numerical images. This study was supported by the Basic Science Research Institute Program, Ministry of Education, BSRI-92-591.

REFERENCES

Barnes, J. & Hut, P. 1986, Nature, 324, 446
Benz, W. 1988, Comp. Phy. Comm., 48, 97
_____. 1990, in Numerical Modelling of Nonlinear Stellar Pulsations: Problems and Prospects, ed. J. R. Buchler (Dordrecht: Kluwer), 269
Benz, W., Bower, R. L., Cameron, A. G. W. & Press, W. H. 1990, ApJ, 348, 647
Courant, R. & Friedrichs, K. O. 1976, Supersonic Flow and Shock Waves (New York: Springer)
Davies, M. B., Benz, W. & Hills, J. G. 1991, ApJ, 381, 449
Durisen, R. H., Gingold, R. A., Tholine, J. E. & Boss, A. P. 1986, ApJ, 305, 281
Evrard, A. E. 1988, MNRAS, 235, 911
Fabian, A. C., Pringle, J. E. & Rees, M. J. 1975, MNRAS, 172, 15
Gingold, R. A. & Monaghan, J. J. 1977, MNRAS, 181, 375
_____. 1980, MNRAS, 191, 897
Goodman, J. & Hernquist, L. 1991, ApJ, 378, 637
Hernquist, L. 1987, ApJS, 64, 715
_____. 1990, J. Comput. Phys. 27, 1
Jernigan, J. D. 1985, in I.A.U. Symposium 113, Dynamics of Star Clusters, ed. J. Goodman & P. Hut (Dordrecht: Reidel), p. 275
Hernquist, L. & Katz, N. 1989, ApJS, 70, 419
Lattanzio, J. C. & Henriksen, R. N. 1988, MNRAS, 232, 565
Lee, H. M. & Ostriker, J. P. 1986, ApJ, 310, 176
Lucy, L. B. 1977, AJ, 82, 1013
McMillan, S. L. W., McDermott, P. N. & Taam, R. E. 1987, ApJ, 318, 261
Monaghan, J. J. 1985, Computer Phys. Rept., 3, 71
_____. 1989, J. Comput. Phys., 82, 1
_____. 1992, Ann. Rev. Astron. Astrophys., 30, 543
Monaghan, J. J. & Gingold, R. A. 1983, J. Comput. Phys., 52, 374
Monaghan, J. J. & Lattanzio, J. C. 1985, A&A, 149, 135
Press, W. H. 1987, in The Use of Supercomputers in Stellar Dynamics, ed. P. Hut & S. L. W. McMillan (Springer Lecture Notes in Physics), 267
Press, W. H. & Teukolsky, S. A. 1977, ApJ, 213, 183
Rasio, F. A. & Shapiro, S. C. 1991, ApJ, 377, 559
Sod, G. A. 1978, J. Comput. Phys., 27, 1
Theuns, T. 1992, A&A, 82, 493
Thomas, P. 1987, Ph. D. thesis, Cambridge Univ.